Available online at www.sciencedirect.com
ScienceDirect
Biochemical and Biophysical Research Communications 362 (2007) 69–74
BBRC
www.elsevier.com/locate/ybbrc

Improving solubility of NR2B amino-terminal domain of *N*-methyl-D-aspartate receptor expressed in *Escherichia coli*

Fui-Mee Ng [a], Wanqin Soh [a], Matthew T. Geballe [b], Chian-Ming Low [a,c,*]

[a] *Department of Pharmacology, Yong Loo Lin School of Medicine, National University of Singapore, Centre for Life Sciences #04-06, 28 Medical Drive, Singapore S117456, Singapore*
[b] *Department of Chemistry, Emory University, Atlanta, GA, USA*
[c] *Neurobiology Programme, Office of Life Sciences, National University of Singapore, Singapore*

Received 13 July 2007
Available online 8 August 2007

Abstract

The amino-terminal domains (ATDs) of *N*-methyl-D-aspartate (NMDA) receptors contain binding sites for modulators and may serve as potential drug targets in neurological diseases. Here, three fusion tags (6×His-, GST-, and MBP-) were fused to the ATD of NMDA receptor NR2B subunit (ATD2B) and expressed in *Escherichia coli*. Each tag's ability to confer enhanced solubility to ATD2B was assessed. Soluble ATD2B was successfully obtained as a MBP fusion protein. Dynamic light scattering revealed the protein (1 mg/ml) exists as monodispersed species at 25 °C. Functional studies using circular dichroism showed that the soluble MBP-ATD2B bound ifenprodil in a dose-dependent manner. The dissociation constants obtained for ifenprodil were similar in the absence (64 nM) and presence (116 nM) of saturating concentration of maltose. Moreover, the yield of soluble MBP-ATD2B is 18 times higher than the refolded 6×His-ATD2B. We have reported a systematic comparison of three different affinity tagging strategies and identified a rapid and efficient method to obtain large amount of ATD2B recombinant protein for biochemical and structural studies.

Keywords: Maltose binding protein; Glutathione-*S*-transferase; NMDA receptor; NR2B; Circular dichroism; *Escherichia coli*

The ionotropic glutamate receptor family is comprised of the *N*-methyl-D-aspartate (NMDA) receptors, α-amino-3-hydroxy-5-methyl-4-isoxazole-propionate receptors, and kainate receptors [1]. The NMDA receptors have been shown to play crucial roles in synaptic plasticity, which underlies learning, memory, and neuronal development [1]. However, prolonged stimulation of NMDA receptors causes excessive Ca^{2+} influx which can lead to neuronal cell death, a mechanism that has been implicated in ischemic stroke, seizures, and head trauma [2–5].

The NMDA receptors exist as hetero-oligomers composed of the obligatory NR1 subunit with NR2, and in some cases NR3 subunits [1,6,7]. All the subunits share a common domain organization: an extracellular amino-terminal domain (ATD), a ligand-binding domain (S1S2), three hydrophobic membrane spanning segments (TM-I, -III, and -IV), a re-entrant pore loop, and an intracellular carboxyl-terminal domain [8,9]. The ATD contains about 400 amino acids proximal to the S1 segment of the ligand binding domain. It exhibits weak structural homology to the bacterial binding protein leucine/isoleucine/valine-binding protein [10]. It has been shown that the ATD forms the binding site of many NMDA receptor modulators such as proton, polyamines, Zn^{2+}, and ifenprodil-like compounds [11–17].

The first atomic crystal structure of NMDA receptors was reported by Furukawa and Gouaux [18], namely the

* Corresponding author. Address: Department of Pharmacology, Yong Loo Lin School of Medicine, National University of Singapore, Centre for Life Sciences #04-06, 28 Medical Drive, Singapore S117456, Singapore. Fax: +65 68737690.
E-mail address: phclowcm@nus.edu.sg (C.-M. Low).

0006-291X/$ - see front matter © 2007 Elsevier Inc. All rights reserved.
doi:10.1016/j.bbrc.2007.07.164

NR1 glycine binding domain. The glutamate binding S1S2 domain of NR2A and the glycine binding S1S2 domain of NR3A were crystallized and solved subsequently [19,20]. Despite the crystal structures of the agonists binding domains of ionotropic glutamate receptors have been solved, there is no crystal structure of the extracellular amino-terminal domain (ATD) of ionotropic glutamate receptors. This is partially attributed to the difficulties in obtaining large amounts of soluble and correctly folded recombinant proteins.

We have previously reported the expression of the ATD of NMDA receptor NR2B subunit (ATD2B) as a 6×His-tagged fusion protein in *Escherichia coli* [21]. The protein was found predominantly in the inclusion bodies. Denaturation followed by refolding yielded low amount of 6×His-ATD2B (~3 mg per litre induction) due to the loss of protein during the refolding stage. The most common strategy to improve the solubility of recombinant proteins expressed in *E. coli* is to attach a solubility-enhancing carrier protein to the target protein [22–24].

Here, we tested the ability of two larger fusion partners, namely glutathione-*S*-transferase (GST) (26 kDa) and maltose binding protein (MBP) (43 kDa) to increase the solubility of the ATD2B. Our results showed that the larger fusion tag, MBP, successfully solubilized the ATD2B. The expression of the ATD2B into the soluble fraction has circumvented the loss of protein during the refolding stage and has resulted in 56 mg yield of purified monodispersed protein per litre of bacteria induction. The soluble MBP-ATD2B binds ifenprodil at nanomolar concentrations.

Materials and methods

Construction of 6×His-, GST-, and MBP-fusion plasmids. The ATD2B gene fragment (Arg27-Arg393; ~1.2 kb) was amplified by polymerase chain reaction using pET30b(+)EG-ATD2B plasmid generated previously as template [21]. Primer pair 5′-CTTAGAATTCCGTTCCCAAAAGA-3′ (sense) and 5′-GCGGCCGCTCGAGTTACTACCGAGGCCACACAT AATAC-3′ (antisense) was designed to generate the amplicon for cloning into pGEX-6P-1 (New England Biolabs, USA) using EcoRI/XhoI multiple cloning sites. Primer pair 5′-CTTAGAATTCCGTTCCCAAAAGA-3′ (sense) and 5′-CTAGTCTAGATTACTACCGAGGCCACAC-3′ (antisense) was used to generate the amplicon for cloning into pMAL-c2(New England Biolabs, USA) using EcoRI/XbaI. The EcoRI/XhoI and EcoRI/XbaI digested amplicons were purified using QIAEXII gel extraction kit (Qiagen, USA) and subcloned into linearized pGEX-6P-1 and pMAL-c2, respectively, using T4 DNA ligase (Promega, USA). The ligated products were transformed into XL2-Blue cells (Stratagene, USA). Positive clones were selected based on restriction enzyme pair digestion of miniprep DNAs that showed ~1.2 kb ATD2B fragment. The full cDNA sequences of ATD2B fragment in both fusion protein plasmids were determined by DNA sequencing and confirmed there was no missense mutation. The plasmids were transformed into BL-21-CodonPlus-RIL cells (Stratagene, USA) according to the manufacturer's instructions.

Optimization of the fusion protein expressions. To perform a 1-litre induction, 100 ml of overnight culture of BL21-CodonPlus-RIL cells transformed with the 6×His-, GST-, and MBP-fusion plasmids were added to 900 ml of fresh Luria–Bertani (LB) media supplemented with their respective antibiotics (100 μg/ml) (kanamycin for pET-30b(+)EG, ampicillin for both pGEX-6P-1 and pMAL-c2). Cells were grown at 37 °C to OD_{600} of ~0.8, after which expression was induced by addition of 1.0 mM IPTG. Induction was performed for 3 h at four different temperatures, 15, 18, 25, and 37 °C. Different protein induction times (3, 5, 7, 9, and 21 h) and IPTG concentrations (0.02, 0.05, 0.1, 0.5, 0.7, and 1.0 mM) were studied. The cells were harvested by centrifugation at 3750 rpm for 15 min at 4 °C and were resuspended in 30 ml of TDE buffer (50 mM Tris–HCl, 0.1 mM DTT, and 0.01 mM EDTA, pH 7.36) supplemented with lysozyme (1 mg/ml), $CaCl_2$ (6 mM), DNase I (5 μg/ml), and phenylmethylsulfonyl fluoride (PMSF) (1 mM). Cell lysis was performed using French Press (Thermo Spectronic) at 15,000 psi on a 40-K cell. The resultant cell lysate was centrifuged for 20 min at 23,000*g* at 4 °C. The supernatant containing the soluble protein was carefully aliquot out while the pellet containing the insoluble protein was resuspended in TDE buffer supplemented with 1 mM PMSF.

Affinity purification of MBP fusion protein. The soluble MBP-ATD2B was loaded into a 20 ml column containing 2 ml amylose resins (New England Biolabs, USA) pre-equilibrated with MBP buffer (200 mM NaCl, 20 mM Tris–HCl, and 1 mM EDTA, pH 8.3) and was allowed to bind for 2 h on a rotary mixer at 4 °C. The column was washed 10 times each with 10 ml of MBP buffer (in presence of 1 mM PMSF). Elution was done using MBP buffer supplemented with 10 mM maltose.

Measurement of soluble protein concentration and dynamic light scattering. The affinity purified MBP-ATD2B protein was concentrated to 10 μM (~1 mg/ml) (Centricon Plus-70, Millipore) as determined by the absorbance at 280 nm and the Bradford protein assay described previously [21]. Dynamic light scattering measurements of MBP-ATD2B protein were made on a DynaPro instrument (Protein Solutions). Proteins samples were centrifuged and 12 μl were aliquot into a quartz cuvette of pathlength 1.5 mm. Measurements were made in duplicates at 25 °C.

Circular dichroism spectroscopy and dose-dependent ligand binding assay. Circular dichroism (CD) measurements were performed at 25 °C on a Jasco J-715 spectropolarimeter [21]. Increasing amounts of ifenprodil (final concentrations: 0.02, 0.05, 0.07, 0.10, 0.50, 1.0, and 5.0 μM) were added to 350 μl of MBP-ATD2B (1 mg/ml). The final change of assay volume was <3%. The samples were scanned from 190 to 250 nm and accumulated 10 times at a resolution of 0.1 nm with a scanning speed of 50 nm/min and sensitivity of 200 mdeg. All of the CD data are expressed as molar ellipticity.

SDS–PAGE, densitometry, and immunoblotting. Proteins were separated by SDS–PAGE and analyzed using Coomassie brilliant blue R-250 as described previously [21]. The densitometry and data analyses were performed using Gel Doc (Bio-Rad, USA) UV spectrophotometer with Quantity One analysis software. Immunoblotting was performed using rabbit polyclonal anti-ATD2B IgG (200 μg/ml, Cat. No. sc-9057, Santa Cruz Biotechnology) 1 in 50,000 dilution as the primary antibody. Detection of the primary antibody was performed using anti-rabbit IgG Horseradish Peroxidase (HRP) (1 mg/ml) followed by ECL Plus Western blotting detection reagent (Amersham Pharmacia, USA).

Modeling of MBP-ATD2B. The model of MBP-ATD2B fusion was built using Maestro (Ver 7.5, Schrödinger, LLC, New York 2006). Structure for open conformation of MBP was taken from 1OMP with water molecules removed [25]. The structure of ATD2B was a homology model built using Prime (Ver 1.5, Schrödinger, LLC, New York 2006). A previously published alignment of ATD2B to mGluR1 [16] provided the basis for a homology model of ATD2B using 1EWK [26] as template. This model was refined through energy minimization and sidechain optimization in Prime. Linker was built using the Maestro build tool.

Results

Cloning and expression of GST-ATD2B fusion protein

The ATD of NR2B gene (amino acids Arg27-Arg393) in fusion with glutathione-*S*-transferase protein, GST-ATD2B, was expressed at a high level in *E. coli* BL21 cells (Fig. 1A). Similar to the 6×His-ATD2B recombinant proteins, most of the GST-ATD2B protein was located in

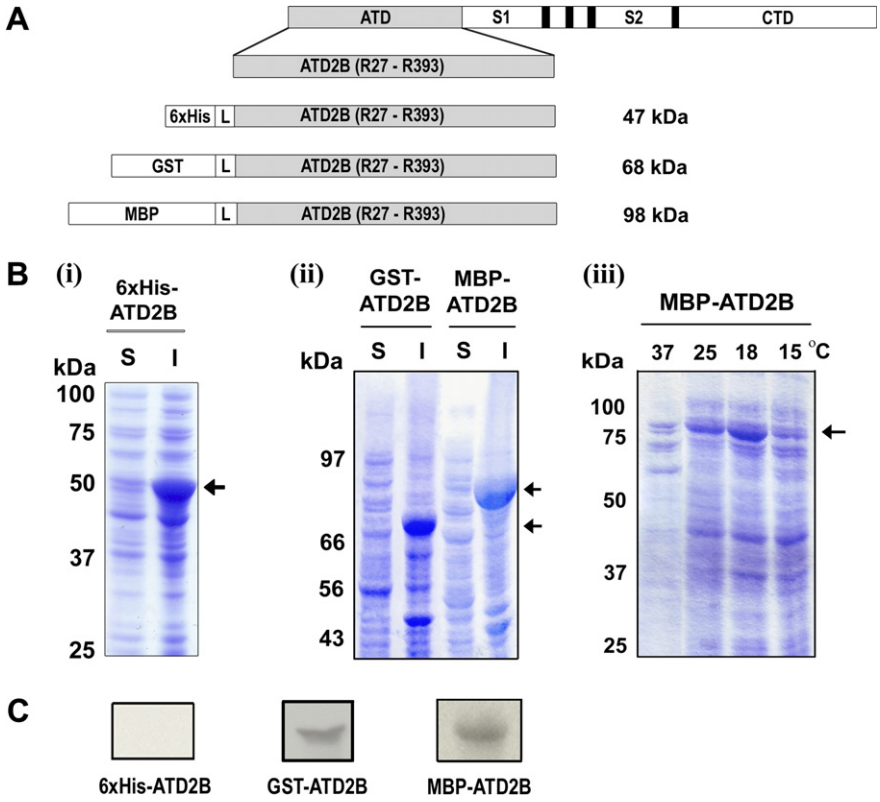

Fig. 1. Expression of the ATD2B fusion proteins. (A) Schematic representation of the ATD2B expression constructs. ATD, amino-terminal domain; S1S2, glutamate binding domains; CTD, C-terminal domain. The ATD (encoding R27-R393) was fused to three different fusion carrier proteins, namely hexahistidine (6×His), glutathione-*S*-transferase (GST) and maltose binding protein (MBP) via linker (L). (B) (i and ii) 6×His-, GST-, and MBP-ATD2B recombinant proteins were separated by SDS–PAGE gel and stained with Coomassie brilliant blue (24 μg protein per lane). S, soluble fraction; I, insoluble fraction. (iii) Optimization of protein induction temperature for MBP-ATD2B (16 μg per lane). (C) Western blot analyses of the soluble fractions of the 6×His-, GST-, and MBP-ATD2B proteins using the anti-ATD2B antibody (24 μg per lane). Fusion proteins of interests were indicated by arrows.

the pellet of bacteria lysate as insoluble inclusion bodies when protein production was induced at 37 °C (Fig. 1B(i) and (ii)). There was very low amount of secreted soluble GST-ATD2B protein that could only be detected by a N-terminal anti-NR2B antibody (sc-9057) as compared to 6×His-ATD2B (<1%) (Fig. 1C). Optimization of the induction temperature (15, 18, and 25 °C) did not help to improve the solubility of GST-ATD2B fusion protein (data not shown).

Cloning and expression of MBP-ATD2B fusion protein

High levels of MBP-ATD2B fusion protein were successfully expressed by inducing BL21 cells that were transformed with pMAL-c2 ATD2B at 37 °C (Fig. 1B(ii)). There was detectable amount of fusion protein secreted as the soluble fraction. The presence and relative amount of the MBP-ATD2B in the soluble fraction was confirmed by immunoblot (Fig. 1C). Lowering the protein induction temperature to 18 °C improved the solubility of MBP-ATD2B to ~60% (Fig. 1B(iii) and Table 1). There were no significant differences in the amount of soluble MBP-ATD2B protein generated between 0.1–1.0 mM IPTG and 3–21 h (data not shown) at 18 °C. Hence, 18 °C/1 mM IPTG/3 h were chosen as the induction conditions to express MBP-ATD2B for all investigations.

Table 1
Estimates of the yields of 6×His-ATD2B and MBP-ATD2B fusion proteins expressed in *Escherichia coli* at optimum induction temperatures of 37 and 18 °C, respectively

Steps	Total fusion protein (mg) per litre induction	
	6×His-ATD2B	MBP-ATD2B
Crude extract	240	800
Inclusion bodies	240	560
Supernatant	0	240
Denaturation	30	—
Affinity purified	9	56
Refolded	3	—

Affinity purification and DLS analysis of MBP-ATD2B

One-step batch purification of the soluble MBP-ATD2B was performed using amylose resin. More than 80% pure MBP-ATD2B were recovered upon elution with 10 mM maltose (Fig. 2A). From one litre induction of *E. coli* BL21 cells, the final yield of purified MBP-ATD2B is 56 mg (23% yield of the cytoplasmic fraction; Table 1).

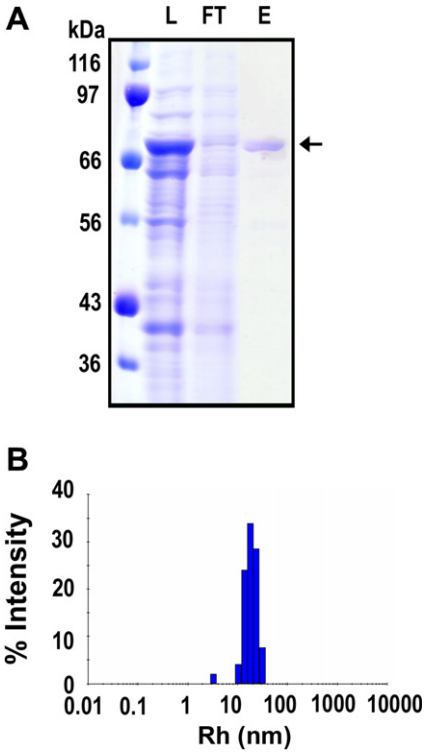

Fig. 2. Affinity purification and DLS characterization of MBP-ATD2B. (A) Commassie blue-stained SDS–PAGE of crude and purified MBP-ATD2B using amylose resin. L, load, FT, flow through; E, eluate of purified MBP-ATD2B. (B) DLS analysis of MBP-ATD2B showed that the protein exists as monomeric species at 25 °C.

The correct translation of ATD2B was confirmed by specific antibodies recognizing MBP (data not shown) and ATD2B as well as amino-terminal peptide sequencing on Factor Xa cleaved MBP-ATD2B. The first eight amino acid residues (underlined) of the Factor Xa-cleaved ATD2B showed that the ATD2B (italic) was translated in frame (IEGR↓ISEF*R*[27]*SQK*[29]) together with MBP linker. MBP-ATD2B protein (1 mg/ml) exhibited monodispersity at 25 °C (Fig. 2B).

Functional characterization of purified MBP-ATD2B

Circular dichroism (CD) is a spectroscopy technique based on the differential absorption of circularly polarized light by chiral molecules. Folded proteins often have α-helices and/or β-sheets which are asymmetrical secondary elements. This property renders proteins as chiral molecules which will display characteristic CD spectra. MBP-ATD2B displayed characteristic α-helices spectrum from 210 to 250 nm wavelengths with a trough at 222 nm (Fig. 3A). In the presence of a ligand for ATD2B, MBP-ATD2B showed shifts in spectra around the 222 nm to a less negative ellipticity (Fig. 3A, non-solid curves). The maximum shifts in ellipticities at 220.5 nm of MBP-ATD2B in the presence of increasing amount of ifenprodil were analyzed. The changes in ellipticities with respect to the apo-MBP-ATD2B were plotted against ifenprodil concentrations (Fig. 3B and C).

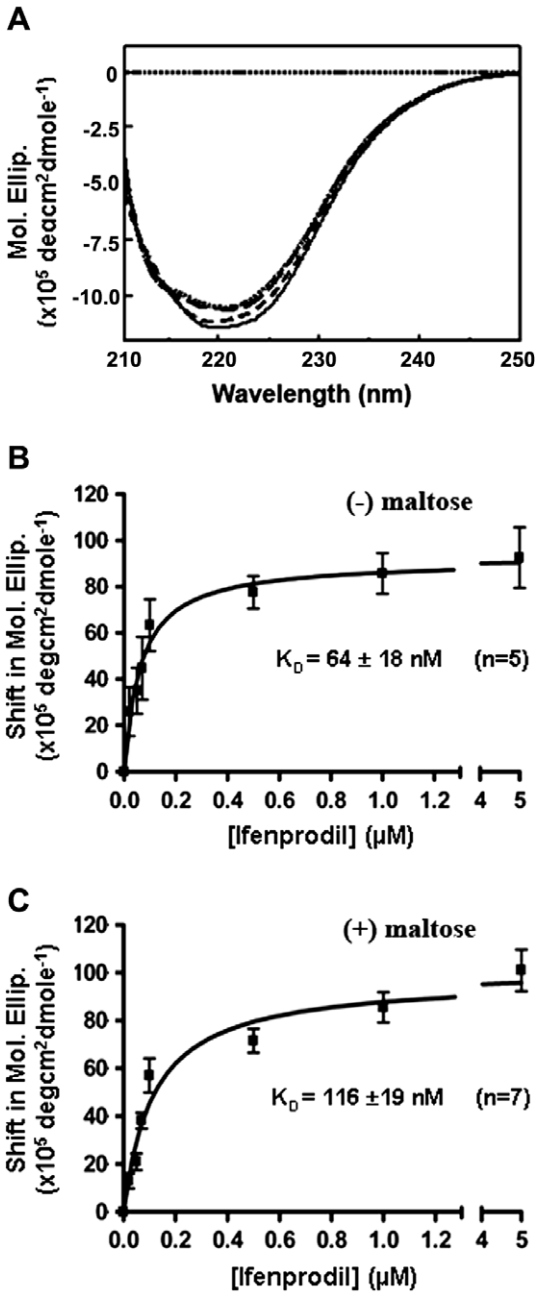

Fig. 3. CD analyses of MBP-ATD2B. (A) CD spectra of MBP-ATD2B protein in the absence and presence of increasing concentrations of ifenprodil. Solid curve represents no ifenprodil, dashed, long dashed and dotted curves represent in the presence of 0.05, 1.0, and 5.0 μM of ifenprodil, respectively. (B) Ifenprodil dose titration curve in the absence of maltose. (C) Ifenprodil dose titration curve in the presence of saturating maltose (30 μM). All error bars are SEM. Numbers in parentheses are the total number of assays from at least two different batches of induced and purified MBP-ATD2B proteins. *X*-axes were truncated between 1.3 and 4.0 μM ifenprodil to illustrate good fitting of dose-titration curves. K_D for maltose on MBP-ATD2B was 1.3 μM ($n = 5$, data not shown) which corroborated with data reported by Telmer and Shilton (1.2 μM) [27].

Since MBP is fused to ATD2B, we performed ifenprodil binding studies on MBP-ATD2B in the absence and presence of maltose. Our results showed that binding of ifenprodil was saturable with a dissociation constant (K_D)

value of 64 ± 18 nM ($n = 5$) in the absence of maltose (Fig. 3B), which corroborated well to that obtained with native rat brain membrane ($K_D = 36.7$ nM) [28]. In the presence of 30 μM maltose to completely saturate the binding site on MBP, ifenprodil bound to the ATD2B with a K_D value of 116 ± 19 nM ($n = 7$) which was comparable to that obtained in the absence of maltose (Fig. 3C).

Discussion

The two most important conclusions to emerge from this study are: (i) that the MBP fusion partner has successfully circumvented the insolubility of the recombinant ATD2B protein, and (ii) that the soluble ATD2B fusion protein binds ifenprodil with K_D values of 64 ± 18 nM and 116 ± 19 nM in the absence and presence of saturating concentration of maltose, respectively.

Our previous attempt to fuse a small, 6×His-tag to the N-terminus of ATD2B led to the production of recombinant protein 6×His-ATD2B that was predominantly trapped in the inclusion bodies [21]. Our result agreed with the observations by Woestenenk et al. that, in general, 6×His-tags (both N- and C-terminal) have a noticeable negative effect on protein solubility [29]. Inclusion bodies can be a good starting point for the purification of proteins since they contain almost pure protein in different states of aggregation [30,31]. However, the loss of 6×His-ATD2B protein during the denaturation and refolding stages led to low yield (3 mg/ml).

Here, we showed that the larger GST- and MBP-fusion tags are more superior to the smaller 6×His-tag in solubilizing the relatively large ATD2B (42 kDa) (Fig. 1C). MBP has better solubilizing characteristics to promote the excretion of ATD2B into the cytoplasm of *E. coli*. Lower protein induction temperatures (<25 °C) further enhance the yield and solubility of the recombinant ATD2B protein [32–34]. Our results agreed with the comparative study conducted by Kapust and Waugh [35] which suggested that MBP is a better fusion partner in improving the solubility of wide array of different proteins compared to GST and theoredoxin.

We showed that soluble MBP-ATD2B was functional in recognizing its exogenous ligand ifenprodil (64 and 116 nM in absence and presence of 30 μM maltose, respectively) which suggested ATD2B was in its native conformation. Although the mechanism by which MBP promotes the solubility and folding of ATD2B is unknown, the N-terminal MBP solubility tag could have provided an optimum context for translation initiation [22,36]. Fig. 4 shows a model of MBP in open conformation fused to ATD2B in an open conformation via a linker polypeptide and the putative ligand binding site.

Our soluble MBP-ATD2B in native conformation provides an alternative to aid biochemical and structure determination of ATD of NR2B subunit of NMDA receptors. Several studies have reported success in crystallizing target proteins fused to large-affinity tags like MBP [37,38].

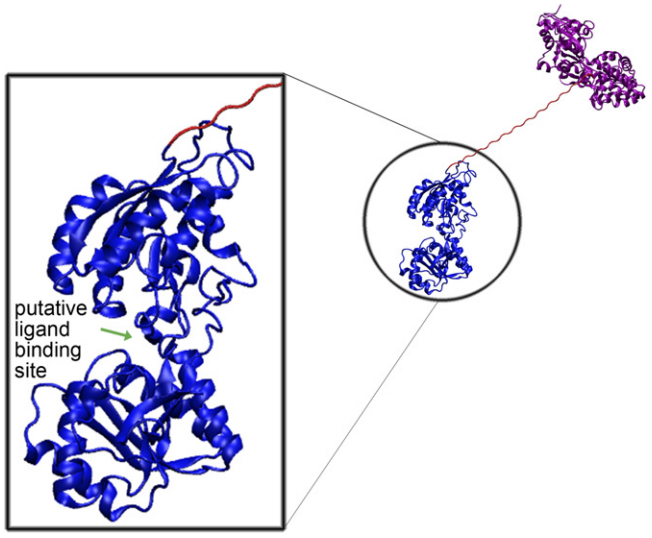

Fig. 4. Model of MBP-ATD2B. MBP (purple) is fused to the ATD2B (blue) via a 24-amino acid "NSSSNNNNNNNNNLGIEGRISEF" linker (orange). The ATD2B is enlarged to highlight the putative ifenprodil binding site at the cleft of the proposed venus flytrap on ATD2B.

Acknowledgments

We are grateful to S.F. Heinemann for sharing cDNA of NR2B (GenBank Accession No. U08261). We thank E. Wong for her suggestions on pMAL-c2 ATD2B and preliminary work. We thank Protein Proteomics Centre, National University of Singapore for the use of DynaPro (Protein Solutions). F.-M.N. is the recipient of a graduate research scholarship from the National University of Singapore. This work was supported by National Medical Research Council (0581/2001), NUS Academic Research Funds (R-184-000-114-112) and Biomedical Research Council (R-184-000-119-305) to C.-M.L.

References

[1] R. Dingledine, K. Borges, D. Bowie, S.F. Traynelis, The glutamate receptor ion channels, Pharmacol. Rev. 51 (1999) 7–61.
[2] D.W. Choi, Glutamate neurotoxicity and diseases of the nervous system, Neuron 1 (1988) 623–634.
[3] U. Dirnagl, C. Iadecola, M.A. Moskowitz, Pathobiology of ischemic stroke: an integrated view, Trends Neurosci. 22 (1999) 391–397.
[4] J.M. Lee, G.J. Zipfel, D.W. Choi, The changing landscape of ischemic brain injury mechanisms, Nature 399 (1999) A7–A14.
[5] T.P. Obrenovitch, J. Urenjak, Is high extracellular glutamate the key to excitotoxicity in traumatic brain injury, J. Neurotrauma 14 (1997) 677–698.
[6] D.R. Madden, The structure and function of glutamate receptor ion channels, Nat. Rev. Neurosci. 3 (2002) 91–101.
[7] M.L. Mayer, Glutamate receptors at atomic resolution, Nature 440 (2006) 456–462.
[8] Z.G. Wo, R.E. Oswald, Unraveling the modular design of glutamate-gated ion channels, Trends Neurosci. 18 (1995) 161–168.
[9] Y. Paas, The macro- and microarchitectures of the ligand-binding domain of glutamate receptors, Trends Neurosci. 21 (1998) 117–125.
[10] P.J. O'Hara, P.O. Sheppard, H. Thøgersen, D. Venezia, B.A. Haldeman, V. McGrane, K.M. Houamed, C. Thomsen, T.L. Gilbert,

E.R. Mulvihill, The ligand-binding domain in metabotropic glutamate receptors is related to bacterial periplasmic binding proteins, Neuron 11 (1993) 41–52.
[11] M.J. Gallagher, H. Huang, D.B. Pritchett, D.R. Lynch, Interactions between ifenprodil and the NR2B subunit of the *N*-methyl-D-aspartate receptor, J. Biol. Chem. 271 (1996) 9603–9611.
[12] T. Masuko, K. Kashiwagi, T. Kuno, N.D. Nguyen, A.J. Pahk, J. Fukuchi, K. Igarashi, K. Williams, A regulatory domain (R1–R2) in the amino terminus of the *N*-methyl-D-aspartate receptor: effects of spermine, protons, and ifenprodil, and structural similarity to bacterial leucine/isoleucine/valine binding protein, Mol. Pharmacol. 55 (1999) 957–969.
[13] S.F. Traynelis, M.F. Burgess, F. Zheng, P. Lyuboslavsky, J.L. Powers, Control of voltage-independent zinc inhibition of NMDA receptors by the NR1 subunit, J. Neurosci. 18 (1998) 6163–6175.
[14] C.-M. Low, F. Zheng, P. Lyuboslavsky, S.F. Traynelis, Molecular determinants of coordinated proton and zinc inhibition of *N*-methyl-D-aspartate NR1/NR2A receptors, Proc. Natl. Acad. Sci. USA 97 (2000) 11062–11067.
[15] F. Perin-Dureau, J. Rachline, J. Neyton, P. Paoletti, Mapping the binding site of the neuroprotectant ifenprodil on NMDA receptors, J. Neurosci. 22 (2002) 5955–5965.
[16] P. Malherbe, V. Mutel, C. Broger, F. Perin-Dureau, J.A. Kemp, J. Neyton, P. Paoletti, J.N.C. Kew, Identification of critical residues in the amino terminal domain of the human NR2B subunit involved in the RO 25-6981 binding pocket, J. Pharmacol. Exp. Ther. 307 (2003) 897–905.
[17] T.W. Rosahl, P.B. Wingrove, V. Hunt, R.L. Fradley, J.M.K. Lawrence, R.P. Heavens, P. Treacey, M. Usala, A. Macaulay, T.P. Bonnert, P.J. Whiting, K.A. Wafford, A genetically modified mouse model probing the selective action of ifenprodil at the *N*-methyl-D-aspartate type 2B receptor, Mol. Cell. Neurosci. 33 (2006) 47–56.
[18] H. Furukawa, E. Gouaux, Mechanisms of activation, inhibition and specificity: crystal structures of the NMDA receptor NR1 ligand binding core, EMBO J. 22 (2003) 2873–2885.
[19] H. Furukawa, S.K. Singh, R. Mancusso, E. Gouaux, Subunit arrangement and function in NMDA receptors, Nature 438 (2005) 185–192.
[20] Y. Yao, M.L. Mayer, Characterization of a soluble ligand binding domain of the NMDA receptor regulatory subunit NR3A, J. Neurosci. 26 (2006) 4559–4566.
[21] E. Wong, F.-M. Ng, C.-Y. Yu, P. Lim, L-H. Lim, S.F. Traynelis, C.-M. Low, Expression and characterization of soluble amino-terminal domain of NR2B subunit of *N*-methyl-D-aspartate receptor, Protein Sci. 14 (2005) 2275–2283.
[22] D.S. Waugh, Making the most of affinity tags, Trends Biotech. 23 (2005) 316–320.
[23] D. Esposito, D.K. Chatterjee, Enhancement of soluble protein expression through the use of fusion tags, Curr. Opin. Biotech. 17 (2006) 353–358.
[24] H. Martin, H. Niklas, B. Susanne, B. Helena, H. Torleif, Rapid screening for improved solubility of small human proteins produced as fusion proteins in *Escherichia coli*, Protein Sci. 11 (2002) 313–321.
[25] A.J. Sharff, L.E. Rodseth, J.C. Spurlino, F.A. Quiocho, Crystallographic evidence of a large ligand-induced hinge-twist motion between the two domains of the maltodetrin binding protein involved in active transport chemotaxis, Biochemistry 31 (1992) 10657–10663.
[26] N. Kunishima, Y. Shimada, Y. Tsuji, T. Sato, M. Yamamoto, T. Kumasaka, S. Nakanishi, H. Jingami, K. Morikawa, Structural basis of glutamate recognition by a dimeric metabotropic glutamate receptor, Nature 7 (2000) 971–977.
[27] P.G. Telmer, B.H. Shilton, Insights into the conformational equilibria of maltose-binding protein by analysis of high affinity mutants, J. Biol. Chem. 278 (2003) 34555–34567.
[28] H. Schoemaker, J. Allen, S.Z. Langer, Binding of [3H]ifenprodil, a novel antagonist, to a polyamine-sensitive site in the rat cerebral cortex, Eur. J. Pharmacol. 176 (1990) 249–250.
[29] E.A. Woestenenk, M. Hammarström, S. van den Berg, T. Härd, H. Berglund, His tag effect on solubility of human proteins produced in *Escherichia coli*: a comparison between four expression vectors, J. Struct. Funct. Genomics 5 (2004) 217–229.
[30] F.A.O. Marston, D.L. Hartley, Solubilization of protein aggregates, Methods Enzymol. 182 (1990) 264–276.
[31] R. Rudolph, H. Lillie, In vitro folding of inclusion body proteins. Folding of acidic fibroblast growth factor, FASEB J. 52 (1996) 49–56.
[32] M. Hammarström, N. Hellgren, S. van den Berg, H. Berglund, T. Härd, Rapid screening for improving solubility of small human proteins produced as fusion proteins in *Escherichia coli*, Protein Sci. 11 (2002) 313–321.
[33] I. Kataeva, J. Chang, H. Xu, C-H. Luan, J. Zhou, V.N. Uversky, D. Lin, P. Horanyi, Z.J. Liu, L.G. Ljungdahl, J. Rose, M. Luo, B-C. Wang, Improving solubility of Shewanella oneidensis MR-1 and *Clostridium thermocellum* JW-20 proteins expressed into *Escherichia coli*, J. Proteome Res. 4 (2005) 1942–1951.
[34] U. Korf, T. Kohl, H. van der Zandt, R. Zahn, S. Schleeger, B. Ueberle, S. Wandschneider, S. Bechtel, M. Schnölzer, H. Ottleben, S. Wiemann, A. Poustka, Large-scale protein expression for proteome research, Proteomics 5 (2005) 3571–3580.
[35] R.B. Kapust, D.S. Waugh, *Escherichia coli* maltose-binding protein is uncommonly effective at promoting the solubility of polypeptides to which it is fused, Protein Sci. 8 (1999) 1668–1674.
[36] D. Sachdev, J.M. Chirgwin, Order of fusions between bacterial and mammalian proteins can determine solubility in *Escherichia coli*, Biochem. Biophys. Res. Commun. 244 (1998) 933–937.
[37] D.R. Smyth, M.K. Mrozkiewicz, W.J. McGrath, P. Listwan, B. Kobe, Crystal structures of fusion proteins with large-affinity tags, Protein Sci. 12 (2003) 131–1322.
[38] Y. Liu, A. Manna, R. Li, W.E. Martin, R.C. Murphy, A.L. Cheung, G. Zhang, Crystal structure of the SarR protein from *Staphylococcus aureus*, Proc. Natl. Acad. Sci. USA 98 (2001) 6877–6882.